Zitierweise: *Angew. Chem. Int. Ed.* **2025**, *64*, e202415272
doi.org/10.1002/anie.202415272

Gene Delivery

Self-Assembled Antibody-Oligonucleotide Conjugates for Targeted Delivery of Complementary Antisense Oligonucleotides

Liujuan Zhou[+], Jie Bi[+], Shenghai Chang[+], Zhaoshuai Bai, Junqi Yu, Ruru Wang, Zhihang Li, Xing Zhang, James J. Chou,* and Liqiang Pan**

Abstract: Antibody-oligonucleotide conjugate (AOC) affords preferential cell targeting and enhanced cellular uptake of antisense oligonucleotide (ASO). Here, we have developed a modular AOC (MAOC) approach based on accurate self-assembly of separately prepared antibody and ASO modules. Homogeneous multimeric AOC with defined ASO-to-antibody ratio were generated by L–DNA scaffold mediated precise self-assembly of antibodies and ASOs. The MAOC approach has been implemented to deliver exon skipping ASOs via transferrin receptor (TfR1) mediated internalization. We discovered an anti-TfR1 sdAb that can greatly enhance nuclear delivery of ASOs. Cryo-EM structure of the sdAb-TfR1 complex showed a new epitope that does not overlap with the binding sites of endogenous TfR1 ligands. In vivo functional analyses of MAOCs with one ASO for single exon skipping and two ASOs for double exon skipping showed that both ASO concentration and exon skipping efficacy of MAOC in cardiac and skeletal muscles are dramatically higher than conventional ASOs in the transgenic human TfR1 mouse model. MAOC treatment was well tolerated in vivo and not associated with any toxicity-related morbidity or mortality. Collectively, our data suggest that the self-assembled MAOC is a viable option for broadening the therapeutic application of ASO via multi-specific targeting and delivery.

Introduction

One of the major advances in gene targeting therapy is the use of anti-sense oligonucleotides (ASOs) to hybridize to a selected region of mRNA to inhibit translation or skip mutated exons for disease treatment.[1] The best-known successes are Eteplirsen (marketed as Exondys 51) and Nusinersen (marketed as Spinraza), both are ASOs for exon skipping and are the first approved disease-targeting drugs used in treating the rare neuromuscular disorders Duchenne muscular dystrophy (DMD)[2] and spinal muscular atrophy (SMA),[3] respectively. In addition to motor neuron diseases, two ongoing ASO-based clinical programs have shown promising results for treating Huntington's disease, in which ASOs were used to reduce pathological protein expression.[4] Additionally, clinical trials of ASOs to treat amyotrophic lateral sclerosis (ALS), Parkinson's disease, and Alzheimer's disease are under way.[5] The notion of using ASO to inhibit target protein expression is highly appealing, as it is, in principle, possible to design relatively short oligonucleotide (16–25 bps) to silence or knock down any genes with good specificity. Furthermore, once ASOs are taken up by cells, they exhibit the property of being long acting.[3b,6]

Major technical challenges, however, have been in achieving in vivo stability and targeted cell delivery of ASO. For addressing in vivo stability, various chemical modifications of the phosphodiester backbone have been developed to render the oligonucleotides resistant to nucleases, such as phosphoramidate,[7] phosphorothioate (PS),[8] and phosphonate analogs.[9] Furthermore, oligonucleotides with natural

[*] L. Zhou,[+] Z. Bai, J. Yu, R. Wang, Z. Li
Assembly Medicine, LLC
Shanghai 201203 (China)
J. Bi,[+] Prof. Dr. L. Pan
College of Pharmaceutical Sciences
Zhejiang University
Hangzhou, 310058 (China)
E-mail: panliqiang@zju.edu.cn
S. Chang,[+] Prof. Dr. X. Zhang
Department of Pathology of Sir Run Run Shaw Hospital, and
Department of Biophysics
Zhejiang University School of Medicine
Hangzhou, 310058 (China)
E-mail: xzhang1999@zju.edu.cn
S. Chang,[+] Prof. Dr. X. Zhang
Center of Cryo Electron Microscopy
Zhejiang University School of Medicine
Hangzhou, 310058 (China)
Prof. Dr. J. J. Chou
Interdisciplinary Research Center on Biology and Chemistry,
Shanghai Institute of Organic Chemistry, State Key Laboratory of Chemical Biology
Chinese Academy of Sciences
Shanghai, 201203 (China)
E-mail: james_chou@mail.sioc.ac.cn
Prof. Dr. J. J. Chou
State Key Laboratory of Chemical Biology
Chinese Academy of Sciences
Shanghai, 201203 (China)
[+] These authors contributed equally to this work

bases but fundamentally different backbone structures have been synthesized, such as phosphorodiamidate morpholino oligomer (PMO)[10] and locked nucleic acid (LNA).[11] These unnatural nucleic acid structures can hybridize with natural DNA and RNA but are not cleavable by natural nucleases or recognized by any of the known innate immune receptors.[12] Currently, most of the approved ASO therapeutics are administered as free or GalNAc3 linked oligonucleotides, or as oligonucleotides encapsulated in lipid nanoparticle (LNP).[13]

Receptor mediated ASO delivery was first demonstrated by conjugating ASO to the triantennary N-acetyl galactosamine (GalNAc3) that can specifically target the asialoglycoprotein receptor.[14] Since the asialoglycoprotein receptor is overexpressed in hepatocytes, GalNAc3-ASOs are generally limited to liver tissue delivery. The receptor mediated delivery was made more general with the use of antibody-oligonucleotide conjugate (AOC), which mimicked the antibody-drug conjugate (ADC). The first demonstration of AOC was that conjugation of thiol-modified oligonucleotides to anti-transferrin receptor 1 (TfR1) antibody modified with maleimide moiety exhibited about 3-fold higher cell association than free oligonucleotides.[15] Subsequent applications of AOCs targeting TfR1 showed >15-fold higher concentration to muscle tissue than unconjugated siRNA.[16] Furthermore, noncovalent charge-mediated antibody-oligonucleotide association has been demonstrated to carry ASO to cell via antibody-receptor interaction and exhibited greater efficacy than free ASOs.[17] These studies suggest that AOC holds great potential in achieving cell selective delivery of ASOs by targeting specific receptor on the cell surface.

In addition to cell specific delivery, there is the need for simultaneously targeting multiple genes in the same cell with an AOC. This need arises from the fact that certain diseases such as DMD involve multiple different mutations across different patient populations. DMD is a devastating monogenic muscle-wasting disorder caused by various large deletions and duplications (79 %) spanning more than one exon in dmd gene.[18] Mutations in the dmd gene result in the absence of functional dystrophin protein, critical for stabilizing the sarcolemma within muscle cells. Exon skipping approaches aim to restore the translation reading frame, yielding a truncated yet functional dystrophin protein.[19] It has been estimated that exon skipping might be applicable to 65 % DMD patients, with the top three skips targeting exons 51 (14.0 %), 53 (10.1 %), and 45 (9.0 %).[18] Most other mutations only individually account for less than 2.0 % of the patients, and no ASOs have been developed for these under-represented populations. Moreover, some DMD patients have two different mutations.

In this study, by exploiting the accurate base pairing property of L–DNA, we implemented a multimeric AOC that is potentially capable of targeting multiple receptors for increasing specificity while simultaneously carrying different ASOs with defined stoichiometric ratio. This AOC is formed with self-assembling modules each comprising a L–DNA sequence and either single-domain antibody (sdAb) for receptor binding or ASO for mRNA targeting, and hence referred to here as modular AOC (MAOC). We found that the self-assembled oligomeric MAOC can be internalized via receptor-mediated endocytosis and its ASO payloads can be released into nucleus for exon skipping of the dystrophin gene both in vitro and in vivo. We also showed that a MAOC that carries two different ASOs can perform double exon skipping of the dystrophin gene in mice. Our results suggest that the MAOC platform has the potential to deliver different ASOs to the same cell for gene therapy in a targeted manner.

Results and Discussion

The Molecular Format of a Self-Assembled Modular AOC

In earlier study, we found that self-assembling L–DNA can be used as a linker to conjugate toxin drug to antibody via either direct formation of chemical bonds or non-covalent L–DNA base pairing.[20] L–DNA has the same base pairing property of regular D-DNA but is not a substrate of any nucleases.[21] Nor it appears to be recognized by receptors of the innate immunity.[22] In that study, the HER2-targeting ADC formed with a tetrameric L–DNA scaffold exhibited favorable receptor-mediated internalization and toxin delivery properties.[20] We hypothesized here that L–DNA conjugated to commonly used ASO such as PS or PMO may also be compatible with self-assembly and receptor-binding mediated internalization of the ASOs. As such, we designed four separate modules that can self-assemble to form AOC complexes with the capability of multi-specific receptor and gene targeting, designated Modular Antibody-Oligonucleotide Conjugate (MAOC).

The designed modules include self-assembling L–DNAs conjugated to either single-domain antibody (sdAb) or 1–2 PMOs (Figure 1). The sdAb was chosen owing to its favorable properties of being small, structurally stable, straightforward for bioconjugation chemistry, and convenient for secreted expression by yeast.[23] One sdAb module is for receptor binding for enhancing cell selectivity and rate of internalization of the MAOC. The other sdAb module is for binding to the human serum albumin (HSA), whose interaction with the neonatal Fc receptor (FcRn) could direct the MAOC to the FcRn-mediated recycling pathway and hence significantly improve the MAOC half-life in vivo. The two ASO modules each contains two PMOs that target the same gene and together can target a set of two different gene fragments. In the molecular format in Figure 1, the four L–DNA chains, designated S1, S2, S3, and S4, have been optimized to self-assemble to only form a tetramer (Figure S1). Given the flexibility of the L–DNA scaffold design, it would be possible to also construct a hexameric assembly that could carry six PMOs targeting three different genes. As a proof-of-concept of the MAOC design, we implemented a self-assembled TfR1-targeting MAOC complex to be applied for exon skipping of the human dystrophin gene, a proven method for treating patients with DMD[2]

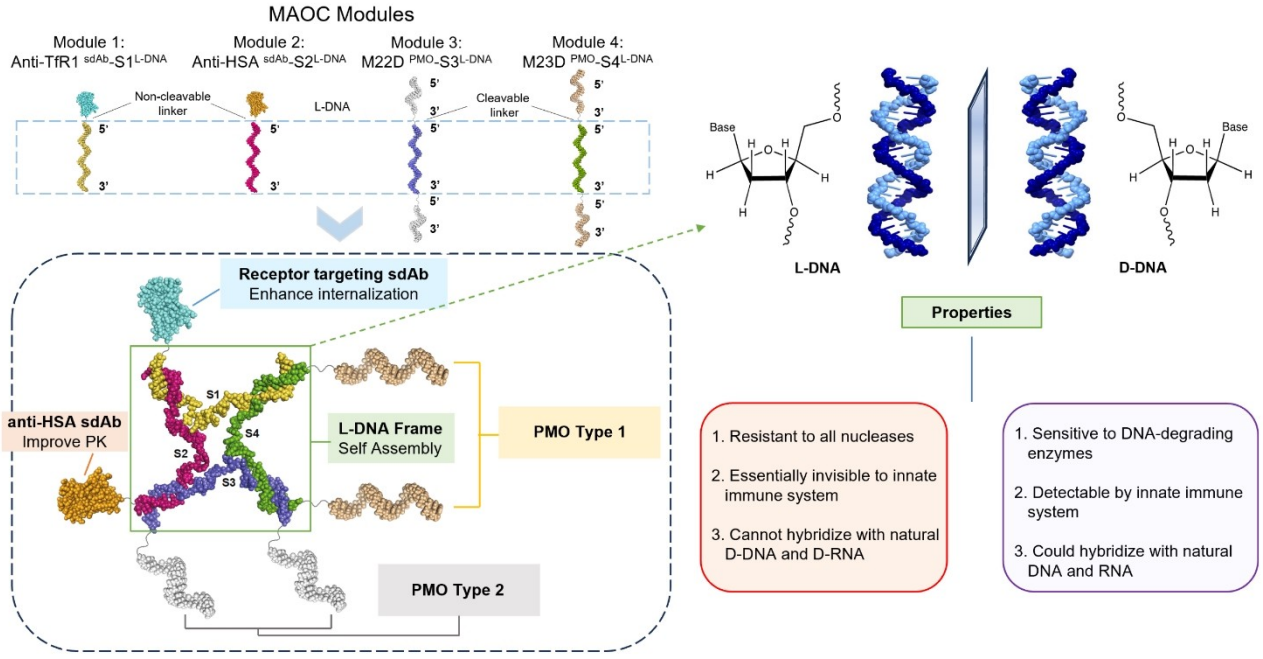

Figure 1. Illustration of the design concept of MAOC. In the figure, D- and L–DNAs are right- and left- handed DNAs, respectively; TfR1 is the transferrin receptor 1; HSA is human serum albumin; PMO is phosphorodiamidate morpholino oligomer; S1 – S4 represent the four L–DNA chains that self-assemble to form a holiday junction like tetramer.

Discovery of an Anti-TfR1 sdAb that Does Not Compete with Transferrin Binding

TfR1 is ubiquitously expressed in most tissue cells with particularly high abundance in fast proliferating cells such as most cancer cells.[24] Owing to its strong ability to internalize, which is an essential step of TfR1-mediated cellular iron uptake, TfR1 has been a favorable receptor target in AOC engineering.[15,16,17b] To find an optimal anti-TfR1 sdAb for carrying ASOs, we used a VHH development strategy involving alpaca immunization with human TfR1 (hTfR1) and yeast display selection of high-affinity VHH binders (Figure S2A). Several sdAb clones were found to bind to hTfR1 with ELISA-derived EC50 of 1–30 nM (Figure S2B). The one that showed the highest stability, cross-species reactivities, and binding affinity in the presence of TfR1 ligand (transferrin) was TfR1-VHH95, with a SPR-derived KD of 0.5 nM (Figure S2C). We also found that a humanized version of TfR1-VHH95 (TfR1-hVHH95) has very similar binding properties as TfR1-VHH95 (Figure S2D).

To further validate specific TfR1 binding, we determined the structure of the anti-TfR1 hVHH95 in complex with hTfR1 at 2.5 Å resolution by cryo-electron microscopy (cryo-EM). The hVHH95 sdAb binds to each protomer of the TfR1 homodimer at the crevice between the apical domain and dimerization domain, resulting in the burial of a solvent-accessible surface area of 739 Å^2 (Figure 2A). Specifically, the complementarity determining region 3 (CDR3) loop plays a pivotal role in recognition, bridging the apical domain with sdAb residues N102 and Y103 and the dimerization domain with E106 and R109 (Figure 2B). In addition, CDR1 T33 and CDR2N52 are proximal to the side chains of TfR1 D245 and Y247, respectively (Figure 2B). The binding mode of hVHH95 is distinct from that of known natural ligands of TfR1 and pathogen-TfR1 recognition (Figure 2C).[25] TfR1 plays a crucial role in cellular iron uptake by binding to holo-transferrin and facilitating its internalization. Importantly, the epitope of hVHH95 is different from the binding sites of transferrin and other endogenous ligands such as hemochromatosis protein (HFE) and heavy-chain ferritin (H–Ft) important for iron homeostasis,[25a,b,c] thus avoiding potential adverse physiological consequences associated with competitive inhibition of endogenous ligand binding. This result is consistent with competitive ELISA assay which showed that VHH95 could bind to hTfR1 in the presence of holo-transferrin or HFE (Figure S3). Another ELISA assay showed that VHH95 could also bind to cyno TfR1 but not mouse TfR1 (Figure S4). Additionally, a tetrameric hVHH95-TfR1 complex, comprising ~20 % of all complexes, is mediated by a homotypic VHH interaction between V93 and L114. To the best of our knowledge, the hVHH95-hTfR1 complex structure provides the first high resolution view of TfR1 binding to an antibody fragment.

Construction of a TfR1-Targeting MAOC for Exon Skipping

Having an optimal anti-TfR1 sdAb for receptor-binding mediated internalization of MAOC, we also developed several anti-HSA sdAbs with cross-species reactivities as a half-life extension module using the same strategy as

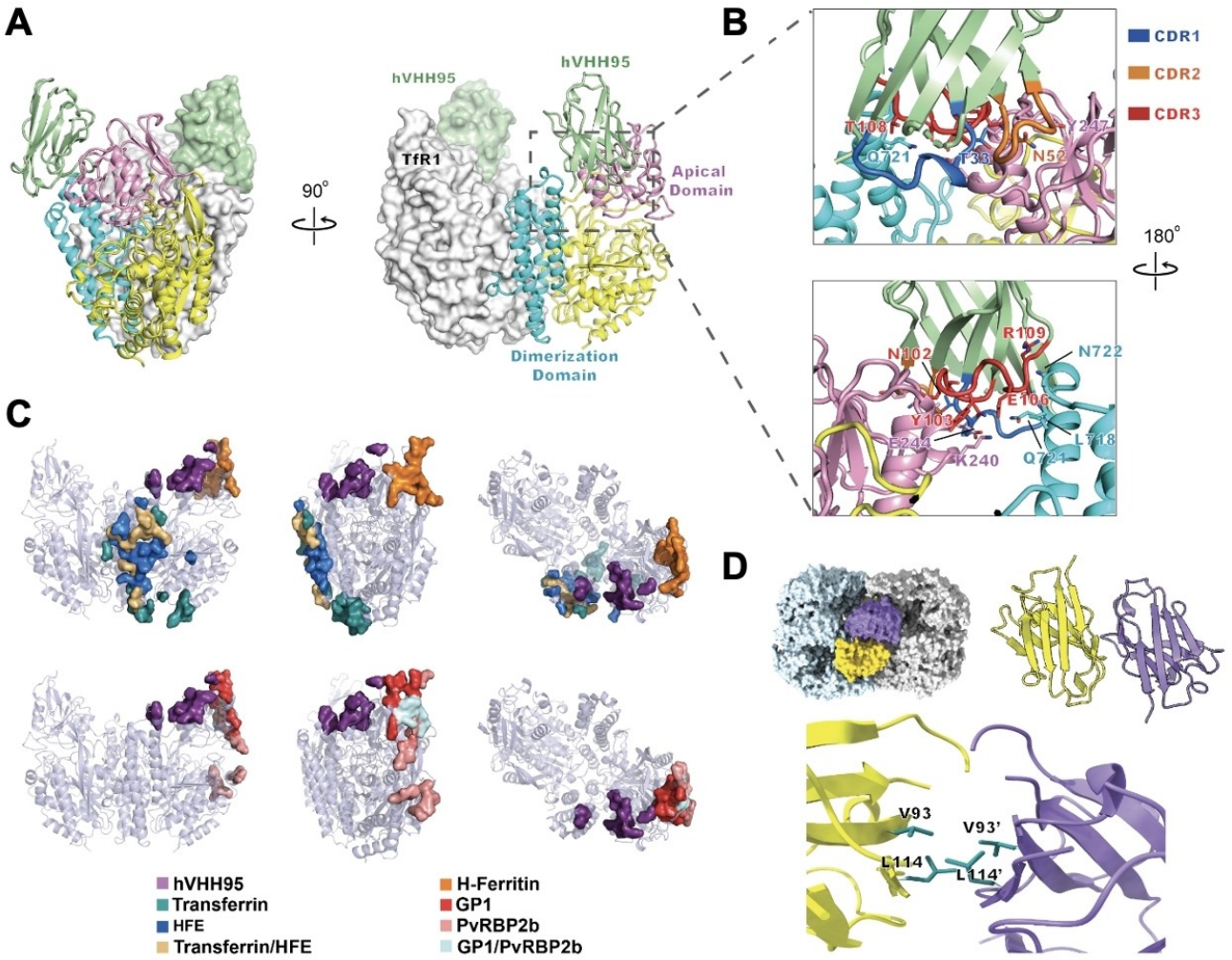

Figure 2. Structure of the hVHH95-hTfR1 complex. A, Cryo-EM structure showing VHH binding to each protomer of the TfR1 dimer. The two protomers are displayed in surface and ribbon representations, respectively. The apical (pink) and dimerization (cyan) domains of the TfR1 are highlighted in the ribbon structure. The VHH is shown in green. B, Detailed views of the hVHH95-TfR1 binding interface showing the three VHH CDR loops in blue (CDR1), orange (CDR2), and red (CDR3). Interacting residues are shown as sticks and labeled with the corresponding CDR colors. C, Comparison of the hVHH95 binding epitope (purple) with the binding sites of known endogenous ligands including transferrin (cyan),[25a] hemochromatosis protein (HFE; blue),[25b] and H-ferritin (orange),[25c] as well as with the binding sites of GP1 from the Machupo virus (red)[25d] and PvRBP2b from P. vivax (pink).[25e] D, Cryo-EM structure of the less populated (~20%) tetrameric hVHH95-TfR1 complex. *Top*: Homodimeric interaction between two hVHH95s, shown in yellow and purple, respectively, brings two TfR1 dimers together to form tetramer. *Bottom*: Detailed view of hydrophobic interactions of V93 and L114 that mediate hVHH95 antiparallel dimerization.

described above (Figure S2A). The ability of anti-HSA sdAbs to extend the in vivo serum half-life was evaluated by fusing the anti-HSA sdAbs to the C terminus of TfR1-VHH95 via a (GGGS)3 linker. The one that showed the best half-life extension property was HSA-VHH118 (Figure S5A). SPR data showed that VHH118 binds to HSA with a KD of 2.82 nM at a neutral pH of 7.4 and 1.62 nM at an endosomal pH of 5.0 (Figure S5B and S5C). Thus, the HSA-VHH118 binding was unaffected by endosomal pH, a precondition for utilizing the FcRn-mediated recycling pathway.

For preparing the sdAb-(L–DNA) conjugates, we employed a previously described method for chemically linking L–DNA and sdAb.[20] In brief, 5'-NH2 modified L–DNA was reacted with the bifunctional linker SM(PEG)2 to generate SM(PEG)2-(L–DNA), which was subsequently conjugated to a C-terminal free Cys of the sdAb under physiological condition and molar ratio of 1:1–1:2 (Figure 3A). The desired reaction product was further purified by sequential steps of nickel affinity chromatography and ion exchange chromatography (Figure 3B). To prepare the PMO-(L–DNA) conjugates, we used PMO containing a cleavable MC–Val-Cit-PAB linker at the 3' end (PMO-MC-vc-PAB) and L–DNA modified with thiol SS–C6 at both 5' and 3' ends (Figure 3C). The cleavable MC–Val-Cit-PAB linker was used to facilitate PMO release from the L–DNA tetrameric scaffold in lysosome.[26] The thiol SS–C6 modified L–DNAs were reduced and mixed with five equivalents of

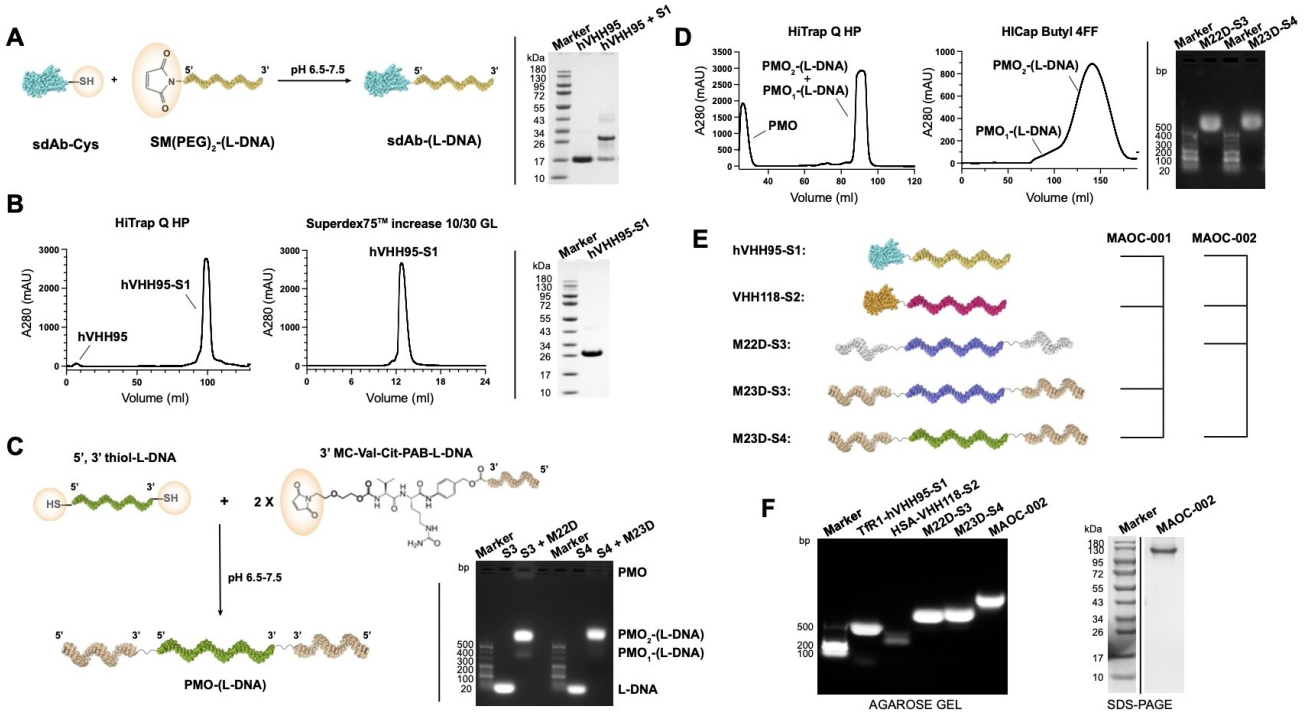

Figure 3. Bioconjugation, purification, and self-assembly of the MAOC modules. A, *Left*: Bioconjugation reaction scheme for generating the sdAb-(L–DNA) module with reactive moieties highlighted in orange. *Right*: SDS-PAGE of hVHH95 and hVHH95 + S1 reaction product showing the conjugation efficiency. B, *Left*: Purification of hVHH95-S1 by ion exchange chromatography (HiTrap Q HP) followed by size exclusion chromatography (Superdex^{TM} 75 Increase 10/300 GL). *Right*: SDS-PAGE of hVHH95-S1 after size exclusion chromatography. C, *Left*: Bioconjugation reaction scheme for generating the PMO-(L–DNA) module with reactive moieties highlighted in orange. *Right*: Agarose gel electrophoresis of PMO + L–DNA reaction products showing the conjugation efficiency. D, *Left*: Separation of PMO-conjugated L–DNA from unconjugated PMO by ion exchange chromatography (HiTrap Q HP) and separation of PMO_2-(L–DNA) from PMO_1-(L–DNA) by hydrophobic interaction chromatography (HICap Butyl 4FF). Right: Agarose gel electrophoresis of M22D-S3 and M23D-S4 showing their purity. E, Schematics of all prepared modules for assembling MAOC-001 and MAOC-002. F, Agarose gel electrophoresis and SDS-PAGE of sdAb-(L–DNA) and PMO-(L–DNA) modules and the assembled MAOCs. The "Marker" and "MAOC-002" lanes are from the same SDS-PAGE gel. We spliced two lanes together to facilitate the molecular weight checking of MAOC-002 sample.

PMO-MC-vc-PAB. Since PMO is significantly more hydrophobic than L–DNA, the L–DNA conjugated to one or two PMOs were separated using hydrophobic interaction chromatography (Figure 3D).

In the current study, the four self-assembling L–DNA chains (S1–S4) were each conjugated to sdAb or PMO using the above conjugation strategies (Figure 3E). The sdAb-(L–DNA) modules include anti-TfR1-S1 (hVHH95-S1) and anti-HAS-S2 (VHH118-S2), for receptor binding and half-life extension, respectively. The PMO-(L–DNA) modules for single exon skipping include M23D-S3 and M23D-S4, where M23D stands for the PMO sequence that blocks exon 23 of the mouse dystrophin gene. In addition, we prepared M22D-S3 and M23D-S4 modules for double skipping of the mouse dystrophin exons 22 and 23, respectively. After preparing the above modules, the MAOC for exon skipping, taking MAOC-002 for example, was constructed by mixing hVHH95-S1, VHH118-S2, M23D-S3, and M23D-S4 at equimolar ratio (Figure 3F).

Internalization and Nuclear Entry Properties of the Self-Assembled MAOC

We first compared MAOC internalization with that of free PMO, sdAb-conjugated PMO, and IgG-conjugated PMO at the same PMO concentration. In order to distinguish MAOC that contains L–DNA from free PMO and other conventional antibody-conjugated PMOs, the PMO (M23D) was labeled with Alexa Fluor 594 at 5' end and the L–DNA chains S2 and S3 were labeled with Cy5.5 at 5' end. The MAOC assembled for this experiment, designated MAOC-003, comprised hVHH95-S1, Cy5.5-S2, Cy5.5-S3, and AF 594 modified PMO-S4. The overall PMO distributions of the four different molecular formats in hTfR1-expressing C2C12 cells were monitored by confocal microscopy over a defined time. Following a 4-hour incubation, we observed that IgG-PMO and MAOC exhibited much more robust internalization than unconjugated and sdAb-conjugated PMOs, with MAOC-003 generating the strongest Alexa Fluor 594 signals inside the nucleus (Figure 4A). The Alexa Fluor 594 and Cy5.5 signals of MAOC-003 colocalized well outside the nucleus (Figure S6A), suggesting that the MAOC-003 was internalized intact. Consistent with the confocal images, the

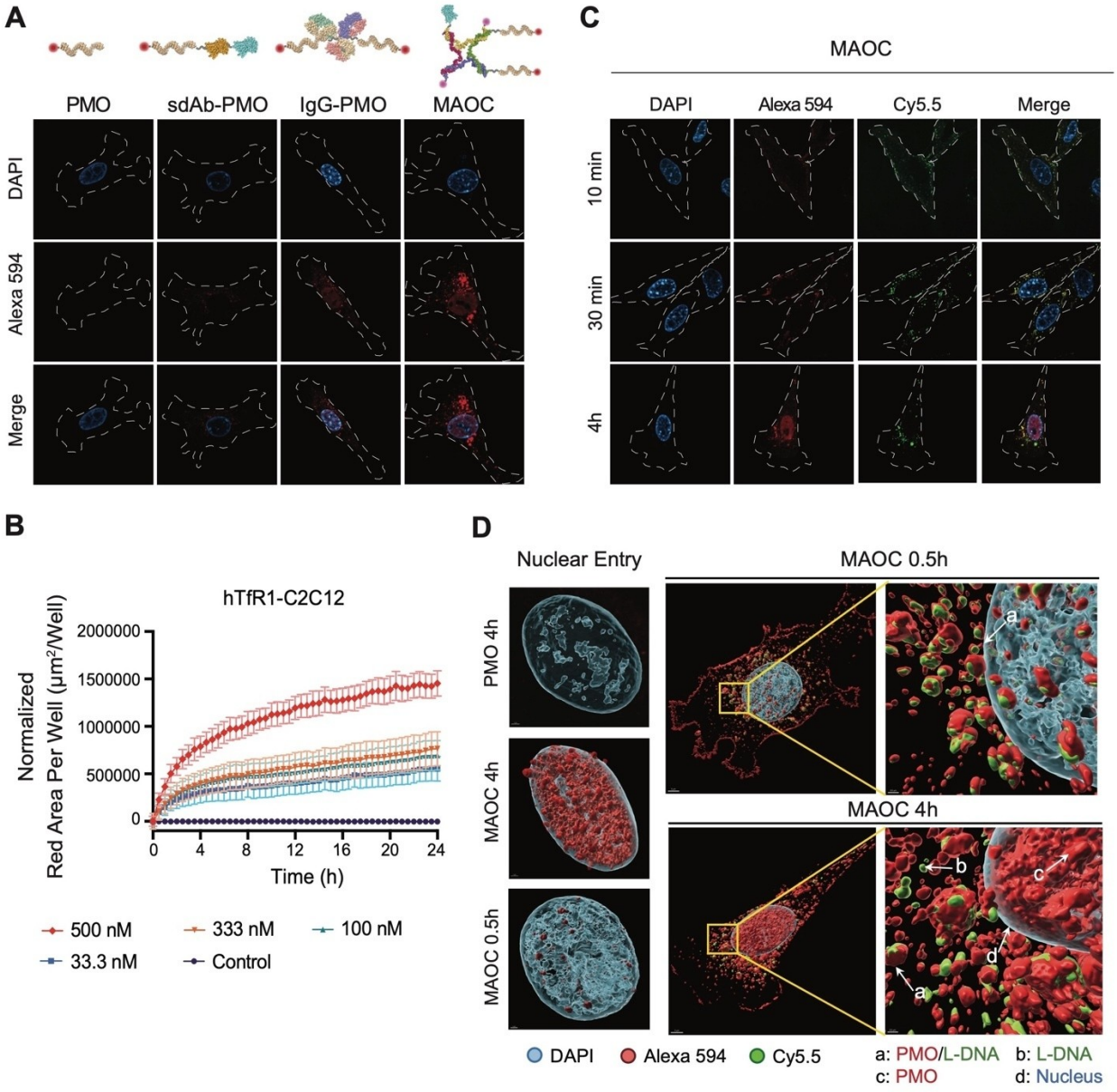

Figure 4. Analysis of internalization and nuclear entry of antibody-PMO conjugates. A, Live-cell imaging of TfR1-humanized C2C12 (hTfR1-C2C12) cells following a 4 h incubation with fluorescently labeled PMO, BsAb-PMO, IgG-PMO, and MAOC. The bispecific antibody, BsAb, is the anti-TfR1 hVHH95 (cyan) fused with the anti-HSA VHH118 (orange); the IgG is the anti-TfR1 monoclonal antibody 13E4;[27] the MAOC-003 is assembled with hVHH95-S1, Cy5.5-S2, Cy5.5-S3, and AF 594 modified PMO-S4. The PMOs are labeled with Alexa Fluor 594 (red), and the L–DNAs, S2 and S3, are labeled with Cy5.5 (assigned to green to be distinct from red). B, Lysosomal entry of hVHH95 labeled with pHrodo™ Red (hVHH95-pHrodo) as reported by low-pH induced red fluorescence in lysosome. The plots are time courses of pHrodo™ fluorescence intensity after treating the hTfR1-C2C12 cells with various concentrations of hVHH95-pHrodo. Data represents mean ± SEM of 3 technical replicates. C, Time-lapse images of the hTfR1-C2C12 cells after incubating with 100 nM of the MAOC in (a) for 10 min, 30 min, and 4 h, showing different time-dependent cellular distribution of the PMO (Alexa Fluor 594) and L–DNA (Cy5.5) components despite being covalently linked initially. D, Nuclear entry of PMO. *Left*: Imaris reconstruction of the DAPI channel showing nuclear entry of PMO following treatment with unconjugated PMO or MAOC. *Right*: 3D reconstruction maps of MAOC-treated hTfR1-C2C12 cells at 0.5 h and 4 h, showing PMO inside the nucleus (red), PMO outside the nucleus (red), L–DNA (green), and the nucleus (light blue).

hVHH95 with a pH-sensitive fluorescent dye (pHrodoTM Red) also showed that the majority of the hVHH95 delivery to late endosome or lysosome have been achieved in 4 hours (Figure 4B). We further examined nuclear entry of MAOC-003 at the 4-hour time point by confocal microscopy. We observed that at 30 min, both Alexa Fluor 594 (L–DNA)

and Cy5.5 (PMO) signals are inside the cell and outside of the nucleus. But, after 4 hours, very robust Alexa Fluor 594 signals appeared inside the nucleus while Cy5.5 remained outside (Figure 4C and Figure S6B), indicating that the PMO components of the MAOC were separated from the L–DNA scaffold for endosomal/lysosomal escape and nuclear entry. Similar results were obtained with super-resolution microscopy using the Airyscan 2 system. To quantify the amount of PMO entry into the nucleus, we employed Imaris software to construct 3D models and calculated the nuclear incorporation efficiency to be approximately 31.4 % by measuring the volume of fluorescence incorporated within the nuclear 3D model (Figure 4D).

Gene Targeting Function of the Self-Assembled MAOC in Vitro and in Vivo

We next investigated the exon skipping property of MAOC in vitro using a mouse myoblast cell line C2C12 that expresses hTfR1. For the exon skipping experiment, MAOC-001 complex (defined in Figure 3E) and M23D (unconjugated PMO) were applied to the cells at increasing dose of 4, 20, 100, and 500 nM. In both cases, the dose described refers to the dose of the PMO component of the test articles. Both MAOC-001 and unconjugated M23D caused partial skipping of exon 23, resulting in a PCR product of 334 bp, which is 213 bp smaller than the endogenous dystrophin gene (Figure 5A and 5B). However, MAOC-001 clearly outperformed M23D in exon skipping efficiency, especially at low PMO concentrations of 4 and 20 nM (Figure 5A and 5B). This result indicates that receptor binding can substantially enhance PMO delivery to the nucleus where splicing occurs, consistent with the above internalization results and previous reports of enhanced delivery of AOCs.[15,16,17]

To examine whether MAOC also shows superior exon skipping in vivo, we administered a single dose of 20 mg/kg unconjugated M23D or MAOC-001 intravenously to transgenic mice with human TfR1 (C57BL/6), followed by tissue-specific analyses of PMO concentration and exon skipping on day 7 and 14 post dosing (Figure 5C and 5D). Again, in this experiment, the dose described refers to the dose of the PMO components in the two test articles (not including the mass from sdAbs, L–DNAs, or linkers). The in vivo data showed an even more drastic improvement of MAOC-001 over unconjugated M23D. Among the tissues analyzed, the enhancement of PMO delivery by MAOC-001 is most pronounced for heart, diaphragm, tibialis anterior, and soleus. For these tissues, the M23D induced exon skipping was too low to be measured on day 14 whereas MAOC-001 induced exon skipping remained at a robust level of 10–30 %. Overall, the PMO concentration and exon skipping delivered by MAOC-001 are correlated, both showing reduced levels from day 7 to 14. Notably, however, the decay of exon skipping is much slower than that of PMO

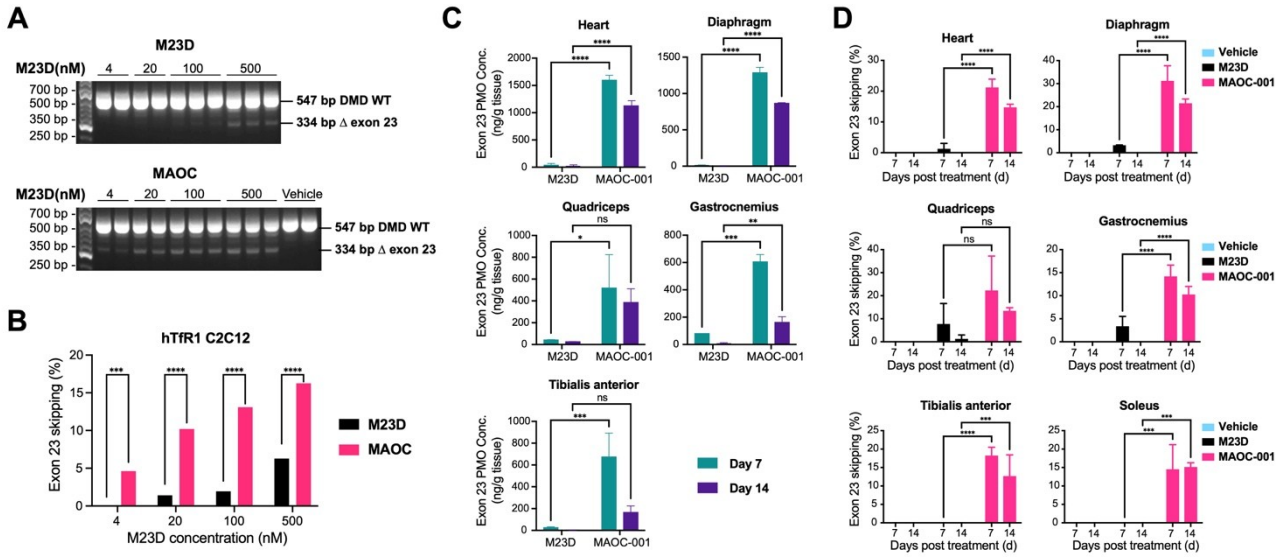

Figure 5. Comparison of in vitro and in vivo efficacies of unconjugated PMO and MAOC-001 in *dmd* exon skipping. A, Nested PCR analysis of *dmd* exon 23 skipping in hTfR1-C2C12 cells treated with unconjugated M23D or MAOC-001 with equivalent amount of M23D. Representative agarose gels showing nested PCR of wild type (547 bp) or exon 23 skipped (334 bp) transcripts. B, Percentage of exon 23 skipping was calculated as the intensity ratio of the 334 bp band to that of the 547 bp band in (A). The band intensities were quantified using the Image Lab software (Bio-Rad). C, Tissue-specific PMO exposure in TfR1-humanized C57BL/6 mice after a single tail vein injection of unconjugated M23D or MAOC-001 with equivalent amount of M23D. PMO exposure was measured using hybridization enzyme-linked immunosorbent assay[28] on days 7 and 14. D, Tissue-specific exon 23 skipping in TfR1-humanized C57BL/6 mice after a single tail vein injection of unconjugated M23D or MAOC-001 with equivalent amount of M23D. Percentage of exon 23 skipping was measured using the same method as in (A) and (B). Significance was determined by two-way ANOVA and Šídák's multiple comparisons test. Data represent mean ± SD. *$P < 0.0332$, **$P < 0.0021$, ***$P < 0.0002$, ****$P < 0.0001$

concentration in gastrocnemius and tibialis anterior as the measured PMO concentration plummeted by more than 3 folds from day 7 to 14 when exon skipping only decreased by ~30 %, suggesting that once the PMO is delivered to the site of action within the cells, its acting time can be much longer than indicated by its half-life in the tissue.

Construction of a Self-Assembled MAOC for Double Exon Skipping

Encouraged by the above in vivo data of the single exon targeting MAOC, we sought to further explore the possibility of precision delivery of two different types of PMOs for skipping two different exons within the same cell. Combinatorial assembly of multiple ASOs for targeted delivery was the original motivation of developing MAOC. By exploiting the modularity of the MAOC approach, we assembled a MAOC complex for dual targeting of exons 22 and 23, designated MAOC-002 (Figure 3E). The purity of the assembled tetrameric MAOC-002 was verified by SDS-PAGE to be >95 % (Figure 3F).

For testing double exon skipping in vivo, the TfR1-humanized C57BL/6 mice were administered a single dose of vehicle, unconjugated M22D + M23D combination (600 nmol/kg each), or MAOC-002 (600 nmol/kg) intravenously, followed by tissue-specific analyses of PMO concentration and exon skipping on day 4, 7, 14, and 21 post dosing. M22D and M23D exposures in muscle tissues were measured using phosphorothioate/DNA reverse complement capture probes for M22D and M23D, respectively. In the MAOC-002 study group, both M22D and M23D were efficiently delivered in all skeletal and cardiac muscle tissues analyzed, and the exposure levels of M22D and M23D were quite close at all time points (Figure 6A), suggesting that MAOC-002 was able to efficiently deliver two different types of PMOs to the same cell. Dramatically lower levels of PMO were measured in the unconjugated M22D + M23D combination group. Moreover, the M22D and M23D exposure levels were not strongly correlated, especially in tissues far from heart such as quadriceps, gastrocnemius, and tibialis anterior (Figure 6A), suggesting that targeting two genes with separate ASOs is much less efficient than using linked ASOs.

Double exon skipping was assessed using nested PCR and agarose gels as described above. We observed both single and double exon skipping occurrences in mice in the two test study groups. The PCR product of the wild-type DMD was dominant with an expected size of 547 bps. Skipping single exon 23 produced a 334 bp PCR product while double skipping of exons 22 and 23 resulted in a product with 188 bps. In addition, the DMD product with single skipping of exon 22 (401 bps) was also observed in some tissues (Figure S7). The sequencing data confirmed the correct sequence in the skipped and wild type products (Figure 6B). We found that in the MAOC-002 study group, very robust double exon skipping could be measured in most of the tissues even on day 21, whereas the unconjugated M22D + M23D combination group showed very minimal double exon skipping in some of the tissues only within 14 days (Figure 6C). Particularly in heart tissue, the double exon skipping activity of MAOC-002 remained in an upward trend from day 4 to 21 despite decreasing PMO concentration. It is worth mentioning that the percentage of double exon skipping among total exon skipping (including single and double exon skipping) in the MAOC-002 study group is higher than that of the unconjugated M22D + M23D combination group (Figure S7), suggesting that MAOC has compelling advantages on precision delivery of multiple oligonucleotides to the same cell.

Conclusion

We have demonstrated that the method of L–DNA mediated self-assembly of modular AOCs can link multispecific sdAbs to multiple types of ASOs with defined stoichiometric ratio, and that the resulting multimeric AOC complex can be delivered in mice for simultaneous skipping of two different exons in the dmd gene for regaining expression of the dystrophin protein. ASO can be used to modulate gene expression through a variety of mechanisms. In the nucleus, it can redirect pre-mRNA polyadenylation to increase gene expression,[29] skip exons to restore expression of mutated genes,[30] or block an exon or intron, which leads to RNA cleavage by RNase H, to downregulate gene expression.[31] In the cytoplasm, ASO hybridizing with mature mRNA can reduce protein expression by disrupting ribosomal assembly at the 5′ cap to inhibit translation[32] or by recruiting RNase H for mRNA cleavage.[31] Given the diverse mechanisms by which ASO can modulate gene expression, its targeted and versatile delivery holds great potential in suppressing difficult-to-target oncogenic proteins such as transcription factors and risk factors in neurodegenerative diseases. The MAOC platform offers a convenient avenue for multispecific targeting of cells and multispecific manipulation of genes for testing preclinical and clinical hypotheses.

The primary challenges of oligonucleotide-based drugs have been productive tissue delivery and uptake efficiency. Many therapeutic applications will also benefit from delivery of multiple different ASOs for simultaneous down regulation of multiple target genes. While the self-assembled L–DNA scaffold affords the opportunity to deliver multiple different ASOs to knock down multiple genes, it was not clear if the large L–DNA tetramer can be used to deliver the hydrophobic PMOs for nuclear entry via the lysosomal pathway. Our internalization experiments have shown that the self-assembled anti-TfR1 MAOC can achieve similar PMO delivery efficiency as the anti-TfR1 IgG-PMO conjugate. Notably, while co-localized L–DNA and PMO fluorescent spots in the context of the intact MAOC were observed in the cytoplasm, only PMO fluorescence was detected within the cell nucleus, indicating very minimal L–DNA translocation into the nucleus. Nanobody conjugation to L–DNA has previously been documented to enhance the resolution of intranuclear detection.[33] Thus, the electrostatic influence on L–DNA nuclear entry is likely negligible. We posit that the barrier to L–DNA nuclear entry is attributed mostly to the structured tetrameric L–DNA

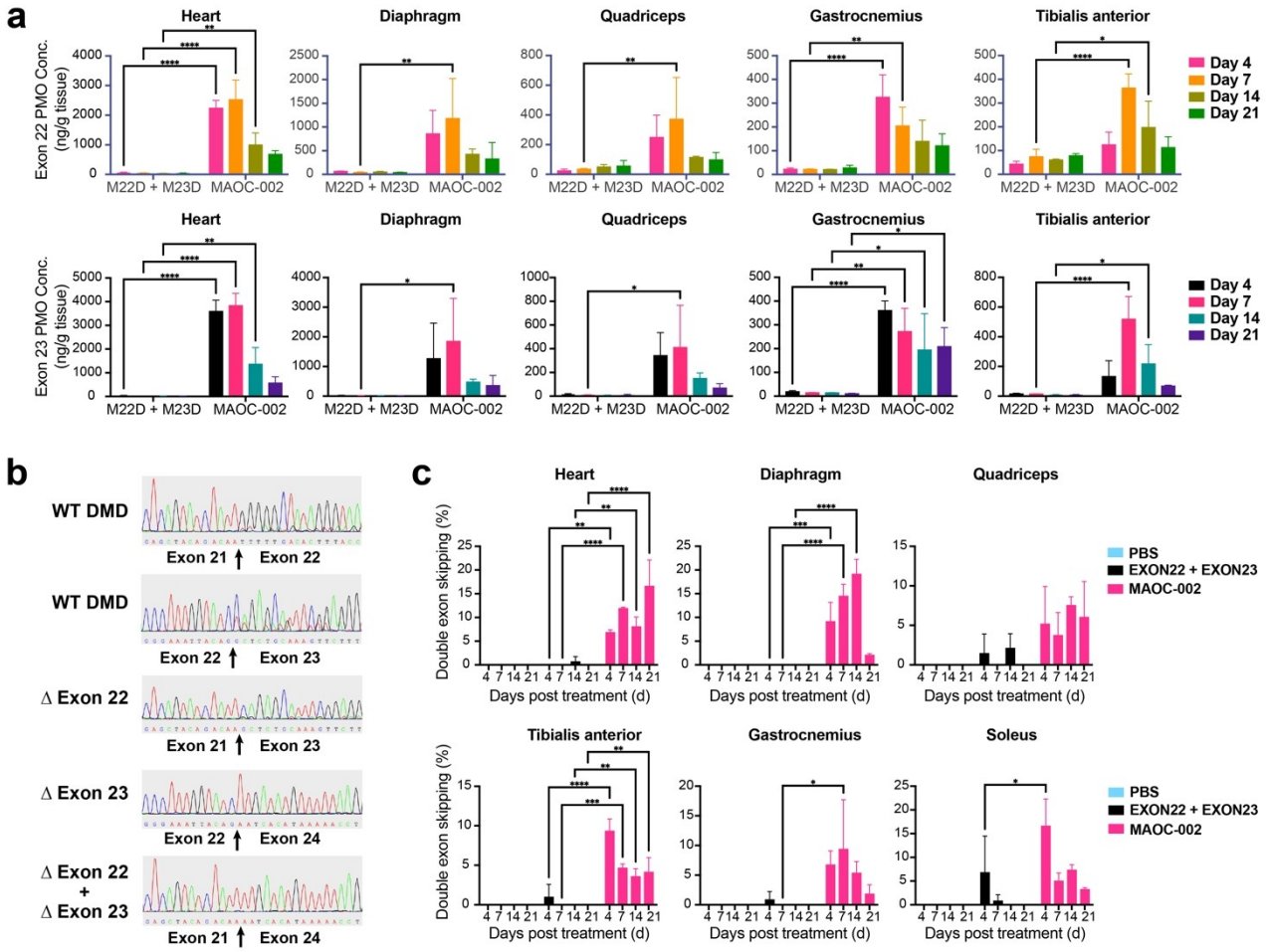

Figure 6. Comparison of in vivo efficacies of unconjugated PMO and MAOC-002 in double *dmd* exon skipping. A, Tissue-specific PMO exposure in TfR1-humanized C57BL/6 mice after a single tail vein injection of vehicle, unconjugated M22D + M23D or MAOC-002 with equivalent amounts of M22D and M23D. PMO exposure was measured using hybridization enzyme-linked immunosorbent assay on days 4, 7, 14, and 21. B, Sequencing data of fragments from the wild type and exon-skipped PCR products of skeletal and cardiac muscles. The arrows indicate the position of skipped exons. C, Tissue-specific exons 22 and 23 skipping in TfR1-humanized C57BL/6 mice after a single tail vein injection of vehicle, unconjugated M22D + M23D or MAOC-002 with equivalent amounts of M22D and M23D. The percentage of double exon skipping was measured using nested PCR and Image Lab software as described above. Significance was determined by two-way ANOVA and Šídák's multiple comparisons test. Data represent mean ± SD. *$P < 0.0332$, **$P < 0.0021$, ***$P < 0.0002$, ****$P < 0.0001$.

scaffold though the structural basis is yet to be characterized. In contrast, PMOs are released from MAOC after linker cleavage and can traverse the NPC unhindered. Therefore, we hypothesize that MAOC undergoes stepwise dissociation akin to a "rocket" during orbit entry, i.e., detachment of the MAOC scaffold during lysosomal escape, allowing free PMOs to enter the nucleus to regulate gene transcription. Moreover, the inclusion of the anti-HSA sdAb module in MAOC is expected to improved plasma pharmacokinetic properties by binding to endogenous albumin during systemic circulation and by FcRn-mediated drug recycling.

The TfR1 binding mediated ASO internalization has been exploited largely in the context of IgG or ligand. Our finding showed that a sdAb binding to TfR1 that does not overlap with any of the natural ligand binding sites can equally facilitate internalization via the TfR1 recycling pathway. Furthermore, the unique epitope of our anti-TfR1 sdAb avoids potential interference with transferrin-mediated iron uptake and other physiological function of the TfR1 receptor. Moreover, during cryo-EM single particle classification, we unexpectedly discovered a tetrameric hVHH95/TfR1 complex (~20 %) mediated by hVHH95 dimerization, suggesting a potential clustering mechanism in receptor-mediated MAOC internalization. The hVHH95 homodimerization could enhance its binding affinity with TfR1 by avidity and thereby promote the intracellular delivery of MAOC by TfR1.

The accurate self-assembling property of the MAOC allows for flexible replacement of its sdAb or ASO components to meet specific requirements of a disease treatment. Moreover, the production of the MAOC is also modularized with each assembling module prepared and preserved separately, which greatly simplifies the making of

highly complicated AOCs, e.g., AOCs with bispecific receptor binding and double or triple gene targeting. The sdAbs of MAOC are produced using the pichia pastoris expression system, which is cheaper to operate than most mammalian expression systems. We also found that the conjugation chemistry for linking L–DNA to sdAbs and PMO are straightforward and efficient, with conjugation yields of 70–90 % and 95–99 %, respectively.

In conclusion, our study demonstrates the feasibility of delivering ASOs in a multispecific receptor- and gene-targeted manner using the MAOC approach. To date, there are 15 FDA approved ASO drugs, all with rare genetic disease indications (ClinicalTrials.gov). In addition to rare diseases, there have been 195 registered clinical trials of ASO drugs for cancer treatments. Although most of these trials did not show significantly improved progress-free survival, complete or partial response have been observed in many patients, i.e., 15 have advanced to phase 2/3 thus far.[34] The potential of ASO in cancer treatment has been limited by two major factors.[34] One is the low specificity and efficiency of drug delivery which, as shown in Figures 4–6, can be partially addressed by antibody conjugation. Since the mode of antibody binding to a receptor could strongly influence its internalization, the receptor binding module of MAOC could be used to screen various sdAb clones to identify the one that supports the highest rate of internalization of the PMO modules. The other is the complex nature of cancer that requires simultaneous targeting of multiple genes within the same cell.[35] In this case, the self-assembling nature and combinatorial flexibility of the MAOC method could afford rapid hypothesis testing of combination gene targeting. Thus, the MAOC represents a versatile research tool for modulating gene expression but also exhibits in vivo properties compatible with future clinical trials.

Supporting Information

The authors have cited additional references within the Supporting Information.[16,17a]

Acknowledgements

We thank Zhaoxiaonan Lin and Wei Yin from the Core Facilities (School of Medicine, Zhejiang University) for their technical support on laser confocal microscopy. This study was supported by research funds from the Assembly Medicine, LLC. J.C. was supported by Shanghai Municipal Science and Technology Major Project (Grant No. 2023000286), CAS grant 2023000040, and Natural Science Foundation of China (Grant No. 82350710799). L.P. was supported by National Key Research and Development Program of China (Grant No. 2023YFC3403900), National Natural Science Foundation of China (Grant No. 82073750), Joint Funds of the National Natural Science Foundation of China (Grant No. U20A20409), State Key Laboratory for Diagnosis and Treatment of Infectious Diseases (Grant No. zz202303). X.Z. was supported by the National Key Research and Development Program of China (Grant No. 2018YFA0507700). S.C. was supported by the National Natural Science Foundation of China (Grant No. 32000844).

Conflict of Interest

L.P. and J.C. are shareholders of Assembly Medicine LLC. L.Z., Z.B., J.Y., R.W., Z.L. are employees of Assembly Medicine LLC. Other authors declare no competing interests.

Data Availability Statement

The data that support the findings of this study are available from the corresponding author upon reasonable request.

Keywords: Multiple Oligonucleotides Delivery · Self-assembly · L–DNA linker · Antibody-Oligonucleotide Conjugates · Transferrin Receptor

[1] a) F. Wang, T. Zuroske, J. K. Watts, *Nat. Rev. Drug Discovery* **2020**, *19*, 441–442; b) B. R. Leavitt, S. J. Tabrizi, *Science* **2020**, *367*, 1428–1429; c) C. Rinaldi, M. J. A. Wood, *Nat. Rev. Neurol.* **2018**, *14*, 9–21; d) C. F. Bennett, A. R. Krainer, D. W. Cleveland, *Annu. Rev. Neurosci.* **2019**, *42*, 385–406; e) C. F. Bennett, H. B. Kordasiewicz, D. W. Cleveland, *Annual Review of Pharmacology and Toxicology* **2021**, *61*, 831–852..

[2] K. R. Lim, R. Maruyama, T. Yokota, *Drug Des. Dev. Ther.* **2017**, *11*, 533–545.

[3] a) C. D. Wurster, A. C. Ludolph, *Ther Adv Neurol Disord* **2018**, *11*, 1756285618754459; b) E. E. Neil, E. K. Bisaccia, *J Pediatr Pharmacol Ther* **2019**, *24*, 194–203.

[4] a) S. J. Tabrizi, B. R. Leavitt, G. B. Landwehrmeyer, E. J. Wild, C. Saft, R. A. Barker, N. F. Blair, D. Craufurd, J. Priller, H. Rickards, A. Rosser, H. B. Kordasiewicz, C. Czech, E. E. Swayze, D. A. Norris, T. Baumann, I. Gerlach, S. A. Schobel, E. Paz, A. V. Smith, C. F. Bennett, R. M. Lane, *N. Engl. J. Med.* **2019**, *380*, 2307–2316; b) S. J. Tabrizi, R. Ghosh, B. R. Leavitt, *Neuron* **2019**, *101*, 801–819.

[5] a) C. J. Mummery, A. Börjesson-Hanson, D. J. Blackburn, E. G. B. Vijverberg, P. P. De Deyn, S. Ducharme, M. Jonsson, A. Schneider, J. O. Rinne, A. C. Ludolph, R. Bodenschatz, H. Kordasiewicz, E. E. Swayze, B. Fitzsimmons, L. Mignon, K. M. Moore, C. Yun, T. Baumann, D. Li, D. A. Norris, R. Crean, D. L. Graham, E. Huang, E. Ratti, C. F. Bennett, C. Junge, R. M. Lane, *Nat. Med.* **2023**, *29*, 1437–1447.b) T. M. Miller, M. E. Cudkowicz, A. Genge, P. J. Shaw, G. Sobue, R. C. Bucelli, A. Chiò, P. V. Damme, A. C. Ludolph, J. D. Glass, J. A. Andrews, S. Babu, M. Benatar, C. J. McDermott, T. Cochrane, S. Chary, S. Chew, H. Zhu, F. Wu, I. Nestorov, D. Graham, P. Sun, M. McNeill, L. Fanning, T. A. Ferguson, S. Fradette, *N. Engl. J. Med.* **2022**, *387*, 1099–1110; c) T. A. Cole, H. Zhao, T. J. Collier, I. Sandoval, C. E. Sortwell, K. Steece-Collier, B. F. Daley, A. Booms, J. Lipton, M. Welch, M. Berman, L. Jandreski, D. Graham, A. Weihofen, S. Celano, E. Schulz, A. Cole-Strauss, E. Luna, D. Quach, A. Mohan, C. F. Bennett, E. E. Swayze, H. B. Kordasiewicz, K. C. Luk, K. L. Paumier, *JCI Insight* **2021**, *6*.

[6] F. Rigo, S. J. Chun, D. A. Norris, G. Hung, S. Lee, J. Matson, R. A. Fey, H. Gaus, Y. Hua, J. S. Grundy, A. R. Krainer, S. P. Henry, C. F. Bennett, *J. Pharmacol. Exp. Ther.* **2014**, *350*, 46–55.
[7] O. A. Patutina, S. K. Gaponova Miroshnichenko, A. V. Sen′kova, I. A. Savin, D. V. Gladkikh, E. A. Burakova, A. A. Fokina, M. A. Maslov, E. V. Shmendel, M. J. A. Wood, V. V. Vlassov, S. Altman, D. A. Stetsenko, M. A. Zenkova, *Proc. Natl. Acad. Sci. USA* **2020**, *117*, 32370–32379.
[8] F. Eckstein, *Nucleic Acid Ther.* **2014**, *24*, 374–387.
[9] a) G. F. Deleavey, M. J. Damha, *Chem. Biol.* **2012**, *19*, 937–954; b) V. K. Sharma, J. K. Watts, *Future Med. Chem.* **2015**, *7*, 2221–2242; c) S. Roy, M. Caruthers, *Molecules* **2013**, *18*, 14268–14284.
[10] a) B. Froehler, P. Ng, M. Matteucci, *Nucleic Acids Res.* **1988**, *16*, 4831–4839; b) E. P. Stirchak, J. E. Summerton, D. D. Weller, *Nucleic Acids Res.* **1989**, *17*, 6129–6141; c) J. Summerton, D. Weller, *Antisense Nucleic Acid Drug Dev.* **1997**, *7*, 187–195.
[11] R. N. Veedu, J. Wengel, *Mol. BioSyst.* **2009**, *5*, 787–792.
[12] a) M. Shadid, M. Badawi, A. Abulrob, *Expert Opin. Drug Metab. Toxicol.* **2021**, *17*, 1281–1292; b) A. A.-O. Kaushal, *Drug Delivery and Translational Research* **2023**, *13*, 2704–2718.
[13] M. Egli, M. Manoharan, *Nucleic Acids Res.* **2023**, *51*, 2529–2573.
[14] a) R. Z. Yu, R. Gunawan, N. Post, T. Zanardi, S. Hall, J. Burkey, T. W. Kim, M. J. Graham, T. P. Prakash, P. P. Seth, E. E. Swayze, R. S. Geary, S. P. Henry, Y. Wang, *Nucleic Acid Ther.* **2016**, *26*, 372–380; b) H. Javanbakht, H. Mueller, J. Walther, X. Zhou, A. Lopez, T. Pattupara, J. Blaising, L. Pedersen, N. Albæk, M. Jackerott, T. Shi, C. Ploix, W. Driessen, R. Persson, J. Ravn, J. A. T. Young, S. Ottosen, *Mol. Ther. Nucleic Acids* **2018**, *11*, 441–454.
[15] I. Walker, W. J. Irwin, S. Akhtar, *Pharm. Res.* **1995**, *12*, 1548–1553.
[16] B. Malecova, R. S. Burke, M. Cochran, M. D. Hood, R. Johns, P. R. Kovach, V. R. Doppalapudi, G. Erdogan, J. D. Arias, B. Darimont, C. D. Miller, H. Huang, A. Geall, H. S. Younis, A. A. Levin, *Nucleic Acids Res.* **2023**, *51*, 5901–5910.
[17] a) E. Song, P. Zhu, S. K. Lee, D. Chowdhury, S. Kussman, D. M. Dykxhoorn, Y. Feng, D. Palliser, D. B. Weiner, P. Shankar, W. A. Marasco, J. Lieberman, *Nat. Biotechnol.* **2005**, *23*, 709–717; b) G. Citro, D. Perrotti, C. Cucco, I. D′Agnano, A. Sacchi, G. Zupi, B. Calabretta, *Proc. Natl. Acad. Sci. USA* **1992**, *89*, 7031–7035.
[18] C. L. Bladen, D. Salgado, S. Monges, M. E. Foncuberta, K. Kekou, K. Kosma, H. Dawkins, L. Lamont, A. J. Roy, T. Chamova, V. Guergueltcheva, S. Chan, L. Korngut, C. Campbell, Y. Dai, J. Wang, N. Barišić, P. Brabec, J. Lahdetie, M. C. Walter, O. Schreiber-Katz, V. Karcagi, M. Garami, V. Viswanathan, F. Bayat, F. Buccella, E. Kimura, Z. Koeks, J. C. van den Bergen, M. Rodrigues, R. Roxburgh, A. Lusakowska, A. Kostera-Pruszczyk, J. Zimowski, R. Santos, E. Neagu, S. Artemieva, V. M. Rasic, D. Vojinovic, M. Posada, C. Bloetzer, P.-Y. Jeannet, F. Joncourt, J. Díaz-Manera, E. Gallardo, A. A. Karaduman, H. Topaloğlu, R. El Sherif, A. Stringer, A. V. Shatillo, A. S. Martin, H. L. Peay, M. I. Bellgard, J. Kirschner, K. M. Flanigan, V. Straub, K. Bushby, J. Verschuuren, A. Aartsma-Rus, C. Béroud, H. Lochmüller, *Hum. Mutat.* **2015**, *36*, 395–402.
[19] T. C. Roberts, M. J. A. Wood, K. E. Davies, *Nat. Rev. Drug Discovery* **2023**, *22*, 917–934.
[20] L. Zhou, F. Yang, Z. Bai, X. Zhou, Z. Zhang, Z. Li, J. Gong, J. Yu, L. Pan, C. Cao, J. J. Chou, *Angew. Chem. Int. Ed. Engl.* **2023**, *62*, e202302805.
[21] a) K. P. Williams, X. H. Liu, T. N. Schumacher, H. Y. Lin, D. A. Ausiello, P. S. Kim, D. P. Bartel, *Proc. Natl. Acad. Sci. USA* **1997**, *94*, 11285–11290; b) M. J. Damha, P. A. Giannaris, P. Marfey, *Biochemistry* **1994**, *33*, 7877–7885; c) L. Pan, C. Cao, C. Run, L. Zhou, J. J. Chou, *Adv. Sci.* **2020**, *7*, 1900973.
[22] M. Boyce, S. Warrington, B. Cortezi, S. Zollner, S. Vauleon, D. W. Swinkels, L. Summo, F. Schwoebel, K. Riecke, *Br. J. Pharmacol.* **2016**, *173*, 1580–1588.
[23] Y. Liu, H. Huang, *Appl. Microbiol. Biotechnol.* **2018**, *102*, 539–551.
[24] a) T. R. Daniels, T. Delgado, J. A. Rodriguez, G. Helguera, M. L. Penichet, *Clin. Immunol.* **2006**, *121*, 144–158; b) M. Uhlén, L. Fagerberg, B. M. Hallström, C. Lindskog, P. Oksvold, A. Mardinoglu, Å. Sivertsson, C. Kampf, E. Sjöstedt, A. Asplund, I. Olsson, K. Edlund, E. Lundberg, S. Navani, C. A. Szigyarto, J. Odeberg, D. Djureinovic, J. O. Takanen, S. Hober, T. Alm, P. H. Edqvist, H. Berling, H. Tegel, J. Mulder, J. Rockberg, P. Nilsson, J. M. Schwenk, M. Hamsten, K. von Feilitzen, M. Forsberg, L. Persson, F. Johansson, M. Zwahlen, G. von Heijne, J. Nielsen, F. Pontén, *Science* **2015**, *347*, 1260419.
[25] a) Y. Cheng, O. Zak, P. Aisen, S. C. Harrison, T. Walz, *Cell* **2004**, *116*, 565–576.b) J. A. Lebrón, M. J. Bennett, D. E. Vaughn, A. J. Chirino, P. M. Snow, G. A. Mintier, J. N. Feder, P. J. Bjorkman, *Cell* **1998**, *93*, 111–123.c) L. C. Montemiglio, C. Testi, P. Ceci, E. Falvo, M. Pitea, C. Savino, A. Arcovito, G. Peruzzi, P. Baiocco, F. Mancia, A. Boffi, A. des Georges, B. Vallone, *Nat. Commun.* **2019**, *10*, 1121.d) J. Abraham, K. D. Corbett, M. Farzan, H. Choe, S. C. Harrison, *Nat. Struct. Mol. Biol.* **2010**, *17*, 438–444.e) J. Gruszczyk, R. K. Huang, L.-J. Chan, S. Menant, C. Hong, J. M. Murphy, Y.-F. Mok, M. D. W. Griffin, R. D. Pearson, W. Wong, A. F. Cowman, Z. Yu, W.-H. Tham, *Nature* **2018**, *559*, 135–139.
[26] J. D. Bargh, A. Isidro-Llobet, J. S. Parker, D. R. Spring, *Chem. Soc. Rev.* **2019**, *48*, 4361–4374.
[27] B. Darimont, V. R. Doppalapudi, R. Johns, *Avidity Biosciences Inc, U.S.* **2021**.
[28] U. Burki, J. Keane, A. Blain, L. O′Donovan, M. J. Gait, S. H. Laval, V. Straub, *Nucleic Acid Ther.* **2015**, *25*, 275–284.
[29] T. A. Vickers, J. R. Wyatt, T. Burckin, C. F. Bennett, S. M. Freier, *Nucleic Acids Res.* **2001**, *29*, 1293–1299
[30] R. Kole, A. R. Krainer, S. Altman, *Nat. Rev. Drug Discovery* **2012**, *11*, 125–140.
[31] X. H. Liang, H. Sun, J. G. Nichols, S. T. Crooke, *Mol. Ther.* **2017**, *25*, 2075–2092.
[32] B. F. Baker, S. S. Lot, T. P. Condon, S. Cheng-Flournoy, E. A. Lesnik, H. M. Sasmor, C. F. Bennett, *J. Biol. Chem.* **1997**, *272*, 11994–12000.
[33] H. J. Geertsema, G. Aimola, V. Fabricius, J. P. Fuerste, B. B. Kaufer, H. Ewers, *Nat. Biotechnol.* **2021**, *39*, 551–554.
[34] H. Xiong, R. N. Veedu, S. D. Diermeier, *Int. J. Mol. Sci.* **2021**, *22*.
[35] a) M. Milella, Z. Estrov, S. M. Kornblau, B. Z. Carter, M. Konopleva, A. Tari, W. D. Schober, D. Harris, C. E. Leysath, G. Lopez-Berestein, Z. Huang, M. Andreeff, *Blood* **2002**, *99*, 3461–3464; b) R. Elez, A. Piiper, B. Kronenberger, M. Kock, M. Brendel, E. Hermann, U. Pliquett, E. Neumann, S. Zeuzem, *Oncogene* **2003**, *22*, 69–80; c) L. Xie, P. E. Bourne, *Front. Pharmacol.* **2015**, *6*, 209; d) J. R. Alvarez-Dominguez, W. Hu, A. A. Gromatzky, H. F. Lodish, *Int. J. Hematol.* **2014**, *99*, 531–541.

Manuscript received: August 11, 2024
Accepted manuscript online: September 26, 2024
Version of record online: November 6, 2024